Title
Cardiac Tissue Architecture and Intracellular Construct Organization and Correlation

Author
Johnsen, Nicholas

Publication Date
2015

Peer reviewed|Thesis/dissertation

UNIVERSITY OF CALIFORNIA,
IRVINE

Cardiac Tissue Architecture and Intracellular Construct Organization and Correlation

THESIS

submitted in partial satisfaction of the requirements
for the degree of

MASTER OF SCIENCE

in Biomedical Engineering

by

Nicholas Eric Johnsen

Thesis Committee:
Assistant Professor Anna Grosberg, Chair
Assistant Professor Susanne M. Rafelski
Assistant Professor Michelle A. Digman

2015

TABLE OF CONTENTS

LIST OF FIGURES

ACKNOWLEDGMENTS

I would like to express appreciation to my principal investigator and thesis committee chair for her guidance and contributions throughout my graduate career. Her efforts to prepare me as a researcher and engineer have significantly added to my experience at UC Irvine. I would also like to thank the other members of my thesis committee for their support and flexibility throughout the writing process.

I would like to thank the Rafelski lab at UC Irvine and especially Irina Mueller for their guidance throughout my research and for confocal imaging support. I also thank Ann Fain for her support with laboratory logistics. I would like to thank Linda McCarthy for training me and managing the cell culture facilities in the core laboratory. I thank Nancy Drew and Jason for your significant contributions to the computational analyses included in this work. I also thank Meghan Knight and Danny Baldo Jr. for your aid in performing primary tissue harvests and training me in preparing tissue samples. I thank Danny Baldo Jr., Meghan Knight, Nancy Drew, and Jason Core for all of the amazing experiences that we have shared working together as labmates. I thank my family and friends for being vital to the continuation of my education and my confidence moving forward. I owe any gains of this journey to each of you.

ABSTRACT OF THE THESIS

Cardiac Tissue Architecture and Intracellular Construct Organization and Correlation

By

Nicholas Eric Johnsen

Master of Science in Biomedical Engineering

University of California, Irvine, 2015

Assistant Professor Anna Grosberg, Chair

The myocardium consists of complex tissue structures that are intricately organized to maintain proper organ function. Though many methods exist for studying cardiac tissue architecture, current in vitro studies do not use consistent approaches for characterizing changes in myocardium structure, which is exist in heart disease. This lack of consistency makes it challenging to compare organization between multiple constructs and tissue types. This work will demonstrate in vitro tools that can quantify the orientational organization of multiple cardiac tissue constructs for comparison as well as quantify the correlation between pairs of constructs. To show the benefits of this method, this study explores the results of the orientational order parameter of multiple spatial and temporal scales and the co-orientational order parameter on engineered cardiac tissues. The results of this study quantitatively show characteristic spatial and temporal scales of organization as well as the level of correlation between pairs of structures. The information gained from this method provides insight into many architectural properties that can be directly compared to data from a variety of other intracellular constructs in normal, diseased, and stem cell-derived cardiac tissues.

Introduction

In heart disease, there is clear evidence of architectural changes in the myocardium, which are likely contributors to poor heart function [1]. The heart muscle is comprised of intricately organized tissues arranged to perform synchronous contractions. Indeed, the various constructs of the cytoskeleton, such as actin fibrils, nuclei, and microtubules, are arranged together, and this correlation is necessary to produce enough force with each contraction of the heart tissue to maintain proper organ function [2-7]. Characterizing the structural features of subcellular constructs can thus introduce a deeper understanding of structure-function relationships in the cardiac environment. Imaging these constructs *in vivo* with sufficient spatial resolution is very challenging, so *in vitro* tools are commonly utilized. A common technique is to engineer cardiac tissues from either cells harvested from neonatal rat ventricular myocytes (NRVM) or stem cell-derived cardiomyocytes, which are still plastic enough to have their myofibrillogenesis guided by external cues [8-10]. It is known that isotropic tissues produce significantly smaller forces compared to anisotropic tissues, which makes them attractive candidates to study the structure-function relationship [11]. In this work, we demonstrate the wide range of application of two parameters in quantifying tissue architecture within anisotropic and isotropic cardiac tissues.

Chapter 1

The Organization and Correlation of Cytoskeletal and Myofibril Constructs

Introduction

As explained in the introduction, cardiac tissue construct architecture is intricately organized to maintain proper organ function. Due to the importance of tissue architecture, it is often visualized for a variety of tissue engineering experiments. However, the quantification of the architecture is not consistent within the field of tissue engineering [12-14]. While a multitude of methods for measuring the orientation of intracellular constructs can be used, it is very challenging to compare tissues from different laboratories unless well-defined parameters are applied to characterize architecture quantitatively. While a variety of metrics have been used [6, 10, 15], they are often underutilized in the field.

As also previously stated, we demonstrate the wide range of application of two parameters in quantifying tissue architecture. The orientational order parameter was used to quantify architecture as a function of spatial scales, to evaluate the efficacy of the code that determined the construct orientations, and to track architecture through myofibrillogenesis. A newer metric, the co-orientational order parameter [16], was used to quantify the correlations in organization of multiple constructs within the tissues. Together, these demonstrate the wide range of applications of organizational parameters in tissue engineering. A wider adaptation of such metrics will make it easier to compare tissues from different origins and groups and accelerate the discoveries in the field.

Materials and Methods

Substrate Preparation

For construct orientation and correlation experiments, glass coverslips (Fisher Scientific Company, Hanover Park, IL) were sonicated in a 95% ethanol solution for 30 minutes for sterility. These coverslips were then coated in polydimethylsiloxane (PDMS) (Ellsworth Adhesives) that was mixed at a 10:1 ratio with curing agent. The coverslips with PDMS coating were cured at 65 ºC overnight.

Extracellular Matrix Printing

Stamp designs were drawn using Adobe Illustrator software (Adobe Systems Inc., San Jose, CA). The designs were etched into 5"x5" chrome with soda-lime glass masks by a third-party vendor (FrontRange Photo Mask Co., Palmer Lake, CO). Silicon wafers were made through SU-8 deposition using the glass masks in the Bio-Organic Nanofabrication Facility (University of California, Irvine). Silicon wafers were placed in Petri dishes and covered in 60-80g of PDMS and curing agent mixed as for coating coverslips in order to create the stamps. The covered wafers were cured at 65 ºC overnight, and then the PDMS was peeled from the wafers. The square regions of the PDMS with patterns were cut out and stored for use as stamps. Prior to applying fibronectin to the coverslips, the coverslips were UVO-treated. The stamps were sonicated and incubated for 1 hour with 0.1 mg/mL drops of fibronectin (Fisher Scientific Company, Hanover Park, IL) placed on top of the patterned faces. Then the coverslips were incubated in 1% pluronic acid solution (5g Pluronics F-127, Sigma Aldrich, Inc., Saint Louis, MO, dissolved in 500 mL sterile water) for 10 minutes in order to block cell adhesion between regions of fibronectin. Coverslips designated for isotropic samples were placed with the PDMS side facing downward on 300 µL drops of 0.05 mg/mL of fibronectin for 10 minutes. After these

steps, both the anisotropic and isotropic coverslips were rinsed in Phosphate Buffered Solution (PBS) (Life Technologies, Carlsbad, CA) three times and kept in PBS until cell seeding.

NRVM Harvest and Seeding

All animal protocols were reviewed and approved by the University of California, Irvine, Institutional Animal Care and Use Committee (Protocol No. 2013-3093). Neonatal Sprague-Dawley rats (Charles River Laboratories, Wilmington, MA), 1-3 days postpartum, were rinsed in 95% ethanol and decapitated. The hearts were rapidly removed and trimmed in Hank's Balanced Salt Solution (HBSS) (Life Technologies, Carlsbad, CA). Once all hearts (10 per harvest) were dissected, they were incubated in a 1 mg/mL trypsin solution (Sigma-Aldrich, Inc., Saint Louis, MO) dissolved in HBSS at 4˚C overnight (12 hours). The trypsin solution was then removed and tissue was neutralized in warmed M199 culture medium (Invitrogen, Carlsbad, CA) supplemented with 10% heat inactivated Fetal Bovine Serum, 10mM HEPES, 20 mM glucose, 2 mM L-glutamine (Life Technologies, Carlsbad, CA), 1.5 μM vitamin B-12 and 50 U/ml penicillin (Sigma-Aldrich Inc., Saint Louis, MO). The media was removed and the tissue was dissociated through several washes of 1 mg/mL collagenase dissolved in HBSS. The collagenase cell solutions were then centrifuged at 1200 rpm for 10 minutes. The supernatant was aspirated and cells were resuspended in chilled HBSS. The HBSS cell solution was centrifuged at 1200 rpm for 10 minutes. The supernatant was aspirated and cells were resuspended in warm 10% FBS M199. The cells were seeded in three pre-plate steps, including 45-minute incubations in two different cell culture flasks and a 40-minute incubation in a third cell culture flask (BD Biosciences, San Diego, CA) in a tissue culture incubator. Cells were counted using a disposable hemocytometer (Fisher Scientific, Waltham, MA) and seeded at a density of 1 million cells per 3 mL.

Endpoint Experiments

The samples for every experiment except for the time point experiments were cultured for 72 hours after seeding. The dead cells were washed off of the samples 24 hours after seeding. To do this, first the media was aspirated off of each sample. Then, warm PBS was used to rinse the samples. After aspirating the PBS, the plate was slammed carefully against the side of the biosafety cabinet to mechanically separate debris from the live cells. This process was completed an additional time and then 10% FBS M199 media was placed back on the samples. The media was replaced by 2% FBS M-199 media 48 hours after seeding to maintain the cardiac myocytes without rapidly increasing the fibroblast population. The samples were fixed 72 hours after seeding.

Time Point Experiments

Time Point Experiments were carried out with the same culture process as the endpoint experiments, but each sample was fixed at a set amount of time after seeding. Once a sample was fixed, all following cell culture steps were omitted.

Fixing and Immunostaining

Live Staining

MitoTracker, which stains for mitochondria and has a low signal-to-noise ratio in fixed tissues, was introduced to tissues prior to fixation to determine the effect of noise on organization data. Just prior to fixation, the tissue culture media was replaced with fresh 2% media with a 100nM dilution of MitoTracker Red CMX Ros (Life Technologies, Carlsbad, CA), and the samples were incubated for 30 minutes in a tissue culture incubator. The tissues were then rinsed 3 times with PBS and left in 2% media without stain for 2 hours to reduce background staining.

Fixing

Before fixing the tissue samples, 4% paraformaldehyde (PFA) (Fisher Scientific Company, Hanover Park, IL) supplemented with 0.001% Triton X-100 (Sigma Aldrich, Inc., Saint Louis, MO) was prepared in PBS and placed in a water bath at 37 ºC along with extra PBS. The plates with the tissue samples were rinsed 3 times with warm PBS and left in the PFA solution for 10 minutes. They were then washed for 5 minutes in PBS three times. The coverslips were left in PBS until they were stained.

Fixed Staining

The samples were each stained for a combination of four of the following: mitochondria and noise using MitoTracker Red CMX Ros as described above, actin (Alex Fluor 488 Phalloidin, Life Technologies, Carlsbad, CA), sarcomeric α-actinin (Mouse Monoclonal Anti-α-actinin, Sigma Aldrich, Inc., Saint Louis, MO), nuclei (4',6'-diaminodino-2-phenylinodole (DAPI), Life Technologies, Carlsbad, CA), and alpha-tubulin (Mouse Monoclonal Anti-α-tubulin and Chicken Polyclonal Anti-α-tubulin, Abcam plc., San Francisco, CA). Secondary staining was done using tetramethylrhodamine-conjugated goat anti-mouse IgG antibody (Alexa Fluor 750 Goat Anti-Mouse, Life Technologies, Carlsbad, CA) and tetramethylrhodamine-conjugated goat anti-chicken IgG antibody (Alexa-Fluor 488 Goat Anti-Chicken, Life Technologies, Carlsbad, CA).

Cover Slide Mounting

Coverslips with stained tissues were mounted onto glass cover slides (VWR, Radnor, PA) for imaging. A drop of ProLong Gold Antifade Reagent (Life Technologies, Carlsbad, CA) was placed atop each cover slide, and the coverslip was placed on the drop with the tissue facing downward. Nail polish (Electron Microscopy Sciences, Hatfield, PA) was then used as sealant along the edge of each coverslip. The sealant was allowed to dry overnight.

Imaging and Image Analysis

Cover slides with immunostained samples were imaged on an IX-83 inverted motorized microscope (Olympus America, Center Valley, PA) mounted with a digital CCD camera ORCA-R2 C10600-10B (Hamamatsu Photonics, Shizuoka Prefecture, Japan) using an UPLFLN 40x oil immersion objective (Olympus America, Center Valley, PA). Ten fields of view were acquired for each sample. Image processing was done using ImageJ software. Image analysis for construct detection, orientational order parameter, and co-orientational order parameter was done using customized MATLAB software (MathWorks, Natick, MA) as previously described [11, 17].

For consistency throughout analysis, local regions were defined as one fourth of a field of view (Fig. S1). Each field of view consisted of an area of 215 μm x 164 μm at 40x magnification. Thus, the local regions considered had an area of approximately 54 μm x 41 μm. Global organization was defined by 10 fields of view at 40x magnification, totaling an area of approximately 3.5 mm^2, where the total area of patterned tissue was 225 mm^2 for anisotropic patterns and 490 mm^2 for isotropic tissues.

Noise Test

Gaussian noise and noise from images of mitochondria stained with MitoTracker were each added to images of actin to test the effect of fluorescent noise on organization data.

Gaussian noise was added to images using the built-in Image J function at standard deviation values of 25 and 300. Noise from MitoTracker images was isolated by subtracting highly contrasted mitochondria image data from the original mitochondria image data. The resulting image was merged with the corresponding actin image from the same field of view and the OOP values were compared to those for the original actin images. Actin images were also merged with MitoTracker noise from other fields of view as an additional condition.

Statistics

To compare the organization of the anisotropic and isotropic tissues, one-way ANOVA was used with the Holm-Sidak post-hoc test, which is commonly used for pairwise comparison of experimental groups. Significance was considered for an unadjusted p-value less than the critical level, which accounts for the number of comparisons. The significance between the COOP, uncorrelated COOP, and correlated COOP values for each pair of constructs analyzed was determined by Student's t-test. A p-value of < 0.05 was considered significant and conversely a p-value of > 0.05 was considered non-significant.

Results

The aim of this work was to demonstrate the utility of applying a variety of metrics to quantify tissue architecture. As a sample system, tissues engineered from neonatal rat ventricular myocytes (NRVMs) were stained for an assortment of intracellular constructs. There exist many methods to quantify orientation of the constructs within *in vitro* tissues, and the metrics discussed in this work can be adapted to work with any of these methods. As an example, the nuclei directions were calculated using a custom code that identified each individual nucleus and its long axis direction (Fig. 1A-B). The orientations of the sarcomeric Z-lines (Fig. 1C-D), actin fibrils (Fig. 1E-F), and tubulin of microtubules (Fig. 1G-H) were calculated using existing codes,

which are similar to codes for detecting ridges of fingerprints [17-19]. To show the versatility of the quantitative metrics, tissues were made to be anisotropic (Fig. 1A, 1C, 1E, 1G) and isotropic (Fig. 1B, 1D, 1F, 1H). As a first general metric of single construct orientation, the orientational order parameter (OOP) was chosen. The OOP has been utilized previously [17, 20-23] and varies from a value of zero in isotropic constructs to one in perfectly aligned constructs. As long as the orientations are known for each coordinate point ($\vec{r}$(x,y)) or individual construct ($\vec{r}_i$), the OOP is easily calculated:

$$\langle T \rangle = \langle 2 \begin{bmatrix} r_x r_x & r_x r_y \\ r_x r_y & r_y r_y \end{bmatrix} - \begin{bmatrix} 1 & 0 \\ 0 & 1 \end{bmatrix} \rangle, \quad (1)$$

$$OOP = \max\big(eigenvalue(\langle T \rangle)\big). \quad (2)$$

The OOP can be calculated for the whole tissue, but it can also provide a measure of organization for different spatial scales (Fig. S1). Therefore, as an example, the OOP was calculated for a range of areas (Fig. 1I-J). The organization of anisotropic tissues is approximately constant over several length-scales (Fig. 1I). However, there is clear evidence of organized patches in isotropic tissues (Fig. 1D). Indeed, the sigmoidal trend allows for identification of a characteristic area (actin: A = 3.6×10^4 μm^2, microtubules: A = 3.8×10^4 μm^2, nuclei: A = 1.8×10^4 μm^2, sarcomeric Z-lines: A = 2.8×10^4 μm^2) which is associated with the tissue becoming spontaneously organized (Fig. 1J). At the smaller length scales, the OOP of the sarcomeres and the nuclei in the isotropic tissues approach their maximal orientations, set by the lines fit to the anisotropic data, on the smallest spatial scales. However, the actin and tubulin constructs do not reach their respective maxima. At the larger length scale, the OOP is relatively constant above ~2×10^4 μm^2 (or above 5 fields of view taken at 40x

magnification combined). It is therefore advisable to use at least 8-10 fields of view for global organization measurements.

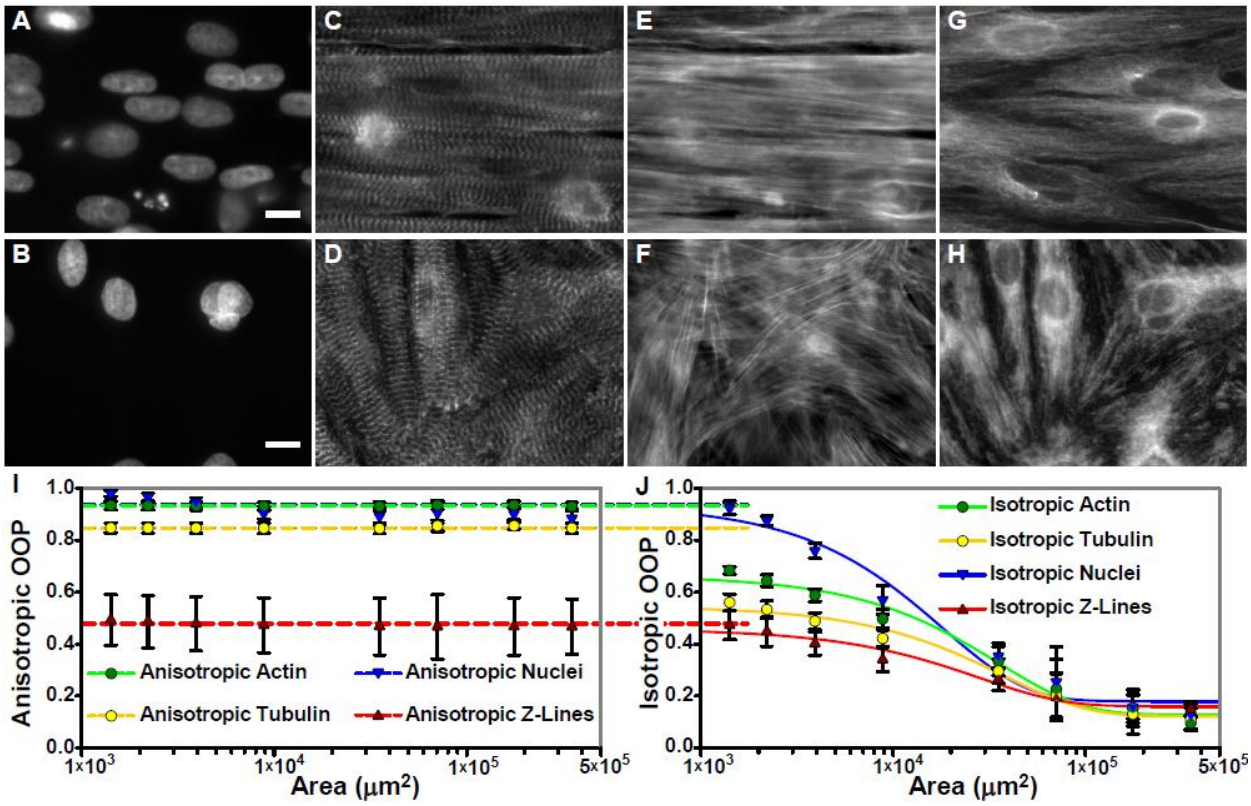

Fig. 1: Orientational order parameter (OOP) analysis over multiple spatial scales for four tissue constructs. (A-H) Immunostain images of anisotropic (A, C, E, G) and isotropic (B, D, F, H) tissues for nuclei (A-B), sarcomeric Z-lines (C-D), actin (E-F), and tubulin (G-H). (I-J) OOP data for anisotropic (I) (N=4) and isotropic (J) (N=8) tissues over multiple spatial scales. Error bars represent the standard deviation of the data. Scale bars 10 μm.

The OOP can also be used to rapidly ensure that the construct detection method is not being biased by experimental noise. To showcase this feature, an image of the actin fibrils in an anisotropic and an isotropic tissue was combined with Gaussian noise and noise from the MitoTracker stain (Fig. 2A-D), and both global and local OOP values were calculated (Fig. 2E). MitoTracker was chosen because the mitochondria images had apparent background noise (Fig. S2). This example showed the insensitivity of the chosen angle detection method to normal noise. However, it also demonstrated a technique to generate example images with too much noise to be analyzed, which are often not obvious a priori (Fig. 2D).

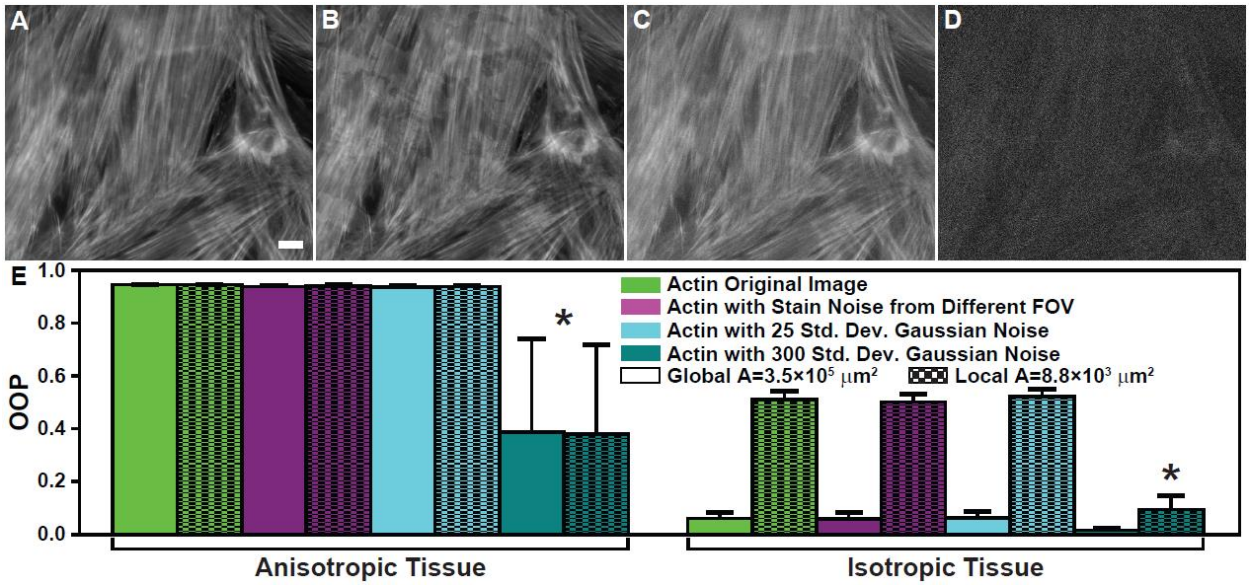

Fig. 2: Stain and artificial noise effects on OOP. (A) Original immunostain image of actin. (B) Immunostain image of actin with MitoTracker noise from a different FOV. (C) Immunostain image of actin with Gaussian noise (standard deviation = 25). (D) Immunostain image of actin with Gaussian noise (standard deviation = 300). (E) OOP data for actin immunostain images treated with each type of noise from anisotropic and isotropic tissues. Error bars represent the standard deviation of the data. Significance was tested within each group (anisotropic (N=3), isotropic (N=4)); global, local), and was $p<0.05$ where labeled with an asterisk. Scale bar 10 μm.

The OOP is a great tool to identify spatial scales as well as to compare different tissue types or to study architectural changes during myofibrillogenesis. For an example, the architectures of both anisotropic (Fig. 3A-D) and isotropic (Fig. 3E-H) tissues were quantified at multiple times post-seeding of the NRVMs (8 hrs, 24 hrs, 48 hrs, 72 hrs). It was found that the global OOP does not change significantly for the isotropic tissues, but it was clear from the data for anisotropic tissues that the organization of the three constructs studied came to equilibrium between 24 and 48 hrs after seeding (Fig. 3I). Interestingly, for a smaller spatial scale ($A \approx 8.9 \times 10^3 \mu m^2$), the nuclei seem to become organized faster than the other constructs (Fig. 3J). This showcased the versatility of the OOP as a parameter. However, it is not capable of quantifying the correlation of orientations for the various constructs within the cells.

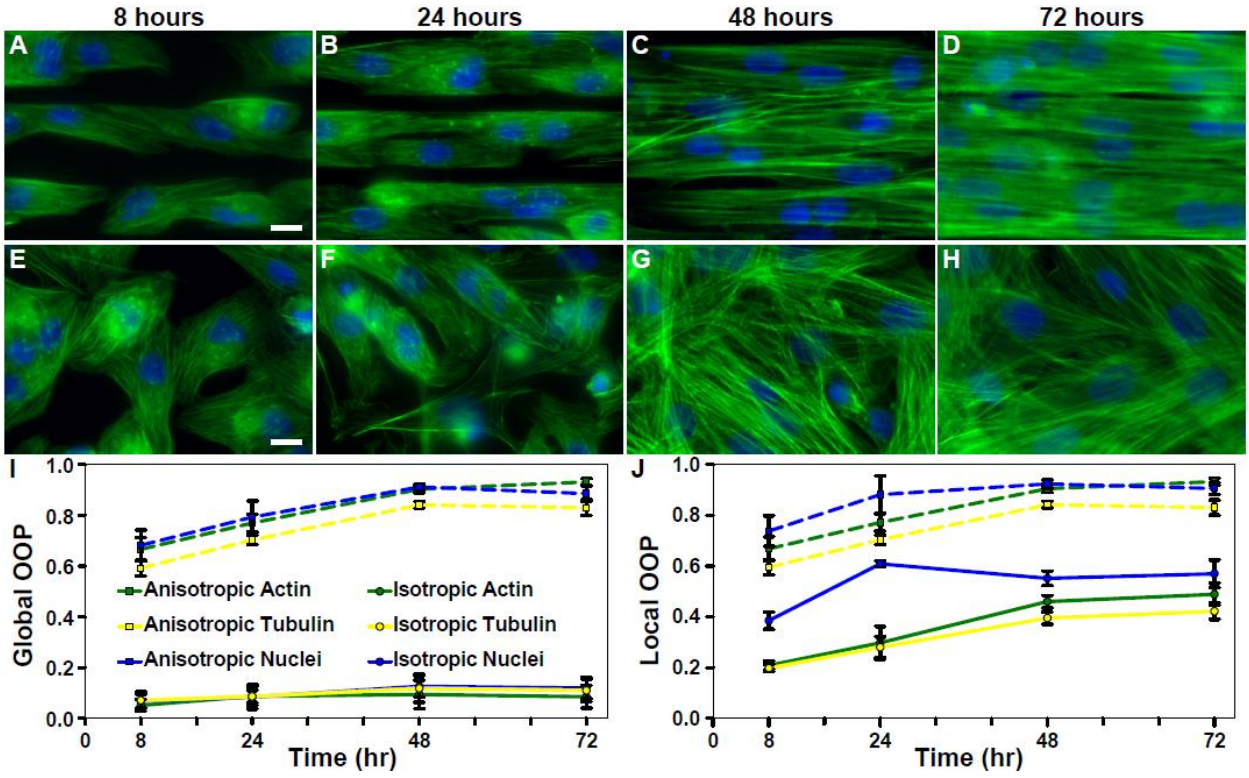

Fig. 3: OOP analysis of constructs over multiple time points post-seeding. (A-H) Immunostain images of anisotropic (A-D) and isotropic (E-H) tissues for actin (green) and nuclei (blue) at 8 hours (A, E), 24 hours (B, F), 48 hours (C, G), and 72 hours (D, H) after tissues were seeded onto substrate. (I-J) Global (I) and local (J) OOP data for the constructs at each time point (Anisotropic: 8hrs N=5, 24hrs N=8, 48hrs N=6, 72hrs N=13; Isotropic: 8hrs N=6, 24hrs N=8, 48hrs N=11, 72hrs N=14). Error bars represent the standard deviation of the data. Scale bars 10 μm.

As the proper correlation is essential for efficient function, the co-orientational order parameter (COOP) tool kit was chosen as the second metric, which would illustrate the quantification of orientation correlations [16]. The COOP quantifies the correlation in orientation of co-localized constructs. While the COOP also varies from zero to one, there exist theoretical low and high limits that represent the uncorrelated and correlated limits for any pair of constructs. Basically, if the COOP is identical to the correlated COOP, then the two constructs are as correlated as possible. Conversely, if the COOP is identical to the uncorrelated COOP, the two constructs are as independent of each other as possible within the tissue:

$$f_{i,x} = \overrightarrow{p_i} \cdot \overrightarrow{q_i} = p_{i,x}q_{i,x} + p_{i,y}q_{i,y} = \cos(\theta) \qquad (3)$$

$$f_{i,y} = |\overrightarrow{p_i} \times \overrightarrow{q_i}| = p_{i,x}q_{i,y} - p_{i,y}q_{i,x} = \sin(\theta) \quad (4)$$

$$T_{PQ} = \langle 2\begin{bmatrix} f_{i,x}f_{i,x} & f_{i,x}f_{i,y} \\ f_{i,x}f_{i,y} & f_{i,y}f_{i,y} \end{bmatrix} - \begin{bmatrix} 1 & 0 \\ 0 & 1 \end{bmatrix}\rangle = \{Mean\ tensor\ of\ the\ system\} \quad (5)$$

$$COOP = max\left[eigenvalue(T_{PQ})\right] \quad (6)$$

$$Uncorrelated\ COOP = \langle 2p_{i,x}^2 - 1\rangle\langle 2q_{i,x}^2 - 1\rangle = OOP_P OOP_Q \quad (7)$$

$$Correlated\ COOP = \frac{\min(OOP_P, OOP_Q)}{\max(OOP_P, OOP_Q)} \quad (8)$$

We explored how the actin fibrils were correlated to the sarcomeric Z-lines, microtubules, and nuclei in NRVM isotropic tissues (Fig. 4A-C). As has been demonstrated previously, the sarcomeric Z-lines were tightly correlated in orientation to the actin fibrils (Fig. 4C(i)), which was expected as both are part of well-developed myofibrils (Fig. 4A). The tubulin of microtubules were not quite maximally correlated with actin fibrils in these tissues (Fig. 4C(ii)), which might be explained by the microtubules and actin fibrils being part of different machinery within the cell. The application of this parameter to the nuclei was more challenging as a direction value was associated with each nucleus instead of each coordinate point (Fig. 4D), as was done for actin images. Hence, it was not clear which direction vectors should be considered as co-localized before their orientations were compared. There were two approaches to address this problem, and the choice dictated the information carried by the parameter. To determine if the orientation of the nucleus is correlated with the gross orientation of the surrounding actin network, the field of view was divided into regions of influence of each nucleus using the Voronoi spaces (Fig. 4D). The average orientation (eigenvector of $\langle T \rangle$ associated with OOP) of the actin was determined for each region (Fig. 4E), and the correlation determined between the

sparse vectors of both constructs (Fig. 4C(iii)). Conversely, to determine if the nucleus direction was tightly correlated with detailed actin orientations, each coordinate point of the Voronoi region was populated with identical vectors of the region's nucleus orientation (Fig. 4F). This new nuclei vector field was compared to the original actin vector field. From performing such a comparison, it was clear that the nuclei orientation was tightly correlated to the gross actin orientation (Fig. 4C(iii)). However, the actin filaments were not correlated to the nucleus individually (Fig. 4C(iv)).

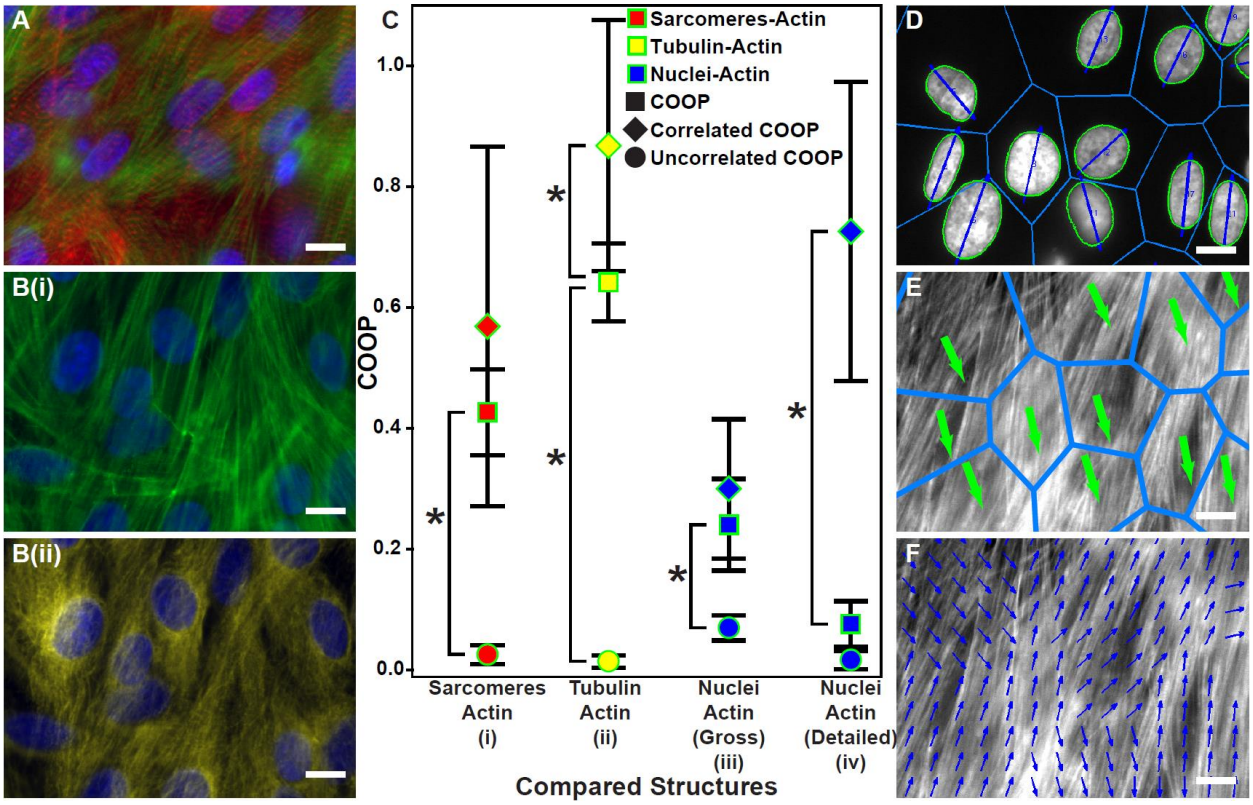

Fig. 4: Co-orientational order parameter analysis for actin against other tissue constructs. (A-B) Immunostain images of sarcomeric Z-Lines (red, A), actin (green, A-B(i)), nuclei (blue, A-B), and tubulin of microtubules (B(ii)). (C) COOP data representing correlation between actin and sarcomeric Z-lines (C(i)) (N=4), tubulin (C(ii)) (N=8), and nuclei (C(iii)-C(iv)) (N=9, N=11). (D) Immunostain image of nuclei with Voronoi diagram (blue mesh) and individual nuclei organization vectors (blue arrows). (E) Immunostain image of actin with Voronoi diagram (blue mesh) and gross actin organization vectors (green arrows). (F) Immunostain image of actin with detailed nuclei organization vectors (blue arrows). Error bars represent the standard deviation of the data. Significance was tested within each pair of constructs between the COOP, Uncorrelated COOP, and Correlated COOP, and was $p<0.05$ where labeled with an asterisk. Scale bars 10 μm.

Discussion

It is imperative to study the relative organization and correlations of various cytoskeletal and myofibril constructs to fully understand cellular architecture and how it is affected by tissue organization. The goals of this study were to perform analysis on cytoskeletal and sarcomere organization and correlation in engineered cardiac tissues and to quantify the dynamic orientational organization of actin, sarcomeres, nuclei, and microtubules during myofibrillogenesis. This work achieved the first goal by showing that a practical method can be utilized to quantify the relative organization between constructs and their correlation within engineered tissues at different length scales. Images of confluent cardiomyocyte monolayers were analyzed to detect the directionality of each structure and to determine OOP values, which have been used previously to represent the level of organization of constructs for specified regions of tissue [24]. These regions were determined to quantify the global, or whole tissue, organization as well as the smaller-scale local organization. The COOP is a new metric that represents the degree of correlation between the orientations of pairs of constructs and was utilized to quantify construct relationships in engineered tissues [16]. This method will improve upon previous methods in terms of consistency and robustness because it can be applied to multiple constructs in differently organized tissues. This research achieved the second goal by showing that the changes in construct orientational organization during myofibrillogenesis can be determined by utilizing the OOP at a series of time points beginning after cell attachment to substrate. This work addresses the lack of quantitative knowledge of subcellular structures and provides a new method for assessing engineered tissues on multiple length scales.

It has not been fully quantified in previous works how tissue organization impacts the quantification of relative orientational organization and correlation in orientation of intracellular

constructs. Examining these properties requires a metric that can be used to analyze a large variety of constructs. It has yet to be shown quantitatively how actin, sarcomere, nuclei, and microtubule constructs develop their orientational organizations during myofibrillogenesis. Throughout myofibrillogenesis, the cytoskeleton remodels actin filaments within sarcomeres. Interactions between the actin and myosin filaments form the highly organized myofibrils [25]. The dynamics of actin filament development throughout this process is still not fully understood for muscle cells [26]. The organization of the nuclei is known to be affected by the microenvironment of tissue monolayers due to direct contact of the nucleus with the surrounding cytoskeleton [27, 28]. Actin filaments apply tension to the nuclei as the cell and tissue morphologies change, which affects the orientation of the nuclei [29]. Microtubules, which are composed of tubulin and other proteins, are spread throughout cardiac myocytes as part of the cytoskeleton, and play a major role in the transport of proteins, lipids, and organelles within individual cells [30]. The relative organization of nuclei and microtubules has yet to be fully quantified in relation to myofibrils and other cytoskeleton components.

No parameter is appropriate for all situations, and therefore it is essential that the limitations are taken into account during data interpretations. None of the parameters would work well if the construct orientation cannot be determined accurately. However, the OOP can be used to identify image qualities that are appropriate for other methods. Still, each parameter also has internal limitations. For instance, the OOP will be the same for an isotropic tissue and for a tissue with multiple primary directions (i.e. perpendicular fibers). However, if the perpendicular fibers are not mixed, the OOP spatial scale study (Fig. 1) would identify such a tissue. Similarly, the COOP does not provide significant information beyond the OOP if there is no statistically significant difference between the correlated and uncorrelated limits. In the

example provided in this work, the COOP was not used with anisotropic tissues as all constructs are correlated to the overall tissue architecture. However, it provides a wealth of information for isotropic tissues (Fig. 4).

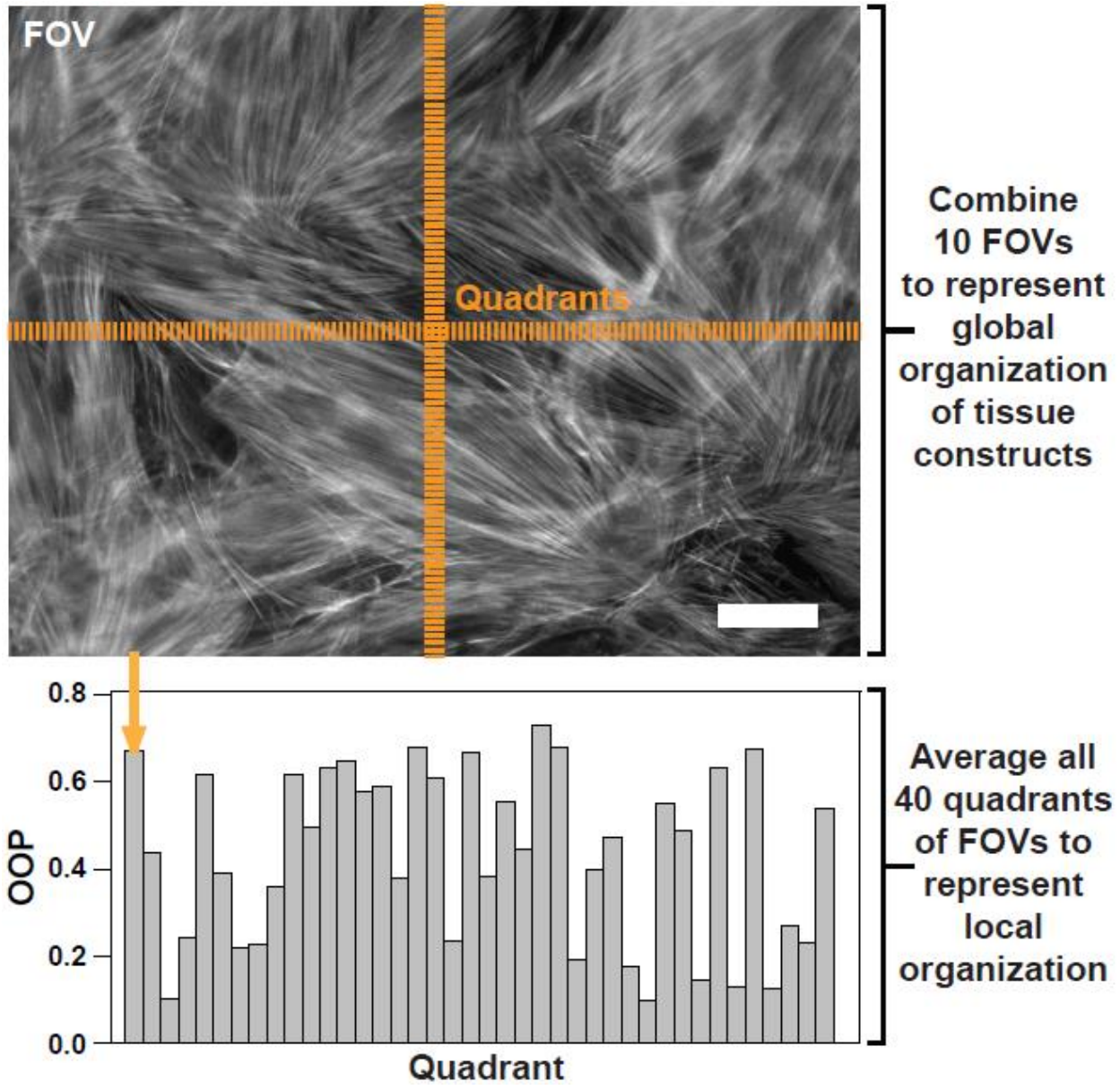

Fig. S1: Determination of local organization. Immunostain image of actin split into four quadrants and OOP data for each quadrant from ten FOVs. Scale bar 25 μm.

Chapter 2

Mitochondrial Organization and Correlation

This chapter will be a brief narrative on studies performed on mitochondria and how they compare to some of the data previously described. Data from other constructs described below are repeated from Chapter 1. These mitochondria studies are not considered to be valid or completed due to issues with the MitoTracker stain and many aspects of the research that go beyond the scope of a Master's Degree plan of study. Still, these results are sufficient to suggest more potential applications for the quantification methods described throughout this thesis.

Introduction

The organization of mitochondria within rat ventricular myocytes is correlated to the organization of sarcomeres and provides localized sites of chemical energy production that are vital for the repeating contractions of heart muscle tissues [31, 32]. Understanding how tissue organization affects this correlation will provide insight into local cardiac energy efficiency changes in disease states where tissue organization is lost. As cardiac myocytes adhere to a surface, they perform myofibrillogenesis and organize the newly developed contractile elements based on the cell morphology. Mitochondria play an essential role in cardiac muscle contraction, and for proper function, mitochondria have to be intricately organized within the cardiac tissues [31-34]. The mitochondria are spread consistently throughout cardiac myocytes, producing chemical energy in the form of adenosine triphosphate (ATP) for use by other organelles, and particularly by the contractile sarcomeres [35-37]. ATP that is formed by ATP synthase within mitochondria phosphorylates creatine, which in turn travels to local contractile structures to phosphorylate adenosine diphosphate into ATP that will be readily available for consumption

[38, 39]. The distribution of mitochondria throughout myocytes provides a consistent supply of ATP at all contractile sites to maintain uniform contraction. However, it has not been fully quantified how tissue organization impacts the correlation between mitochondrial and sarcomere organization. Previous works have investigated the exact organization of mitochondria within cardiac muscle cells, but only for single cells that are not cultured as parts of tissues [35, 36].

Results

For a preliminary understanding of mitochondrial organization, NRVM tissue monolayers stained for mitochondria were imaged and analyzed (Fig. 5A-B). As seen with the other constructs, the OOP of the mitochondria is the same on two different spatial scales within the anisotropic tissues, where it is very different in isotropic tissues (Fig. 5C). This suggests that the effects of tissue organization on mitochondrial organization may be similar to the effects on the cytoskeletal and myofibril organizations.

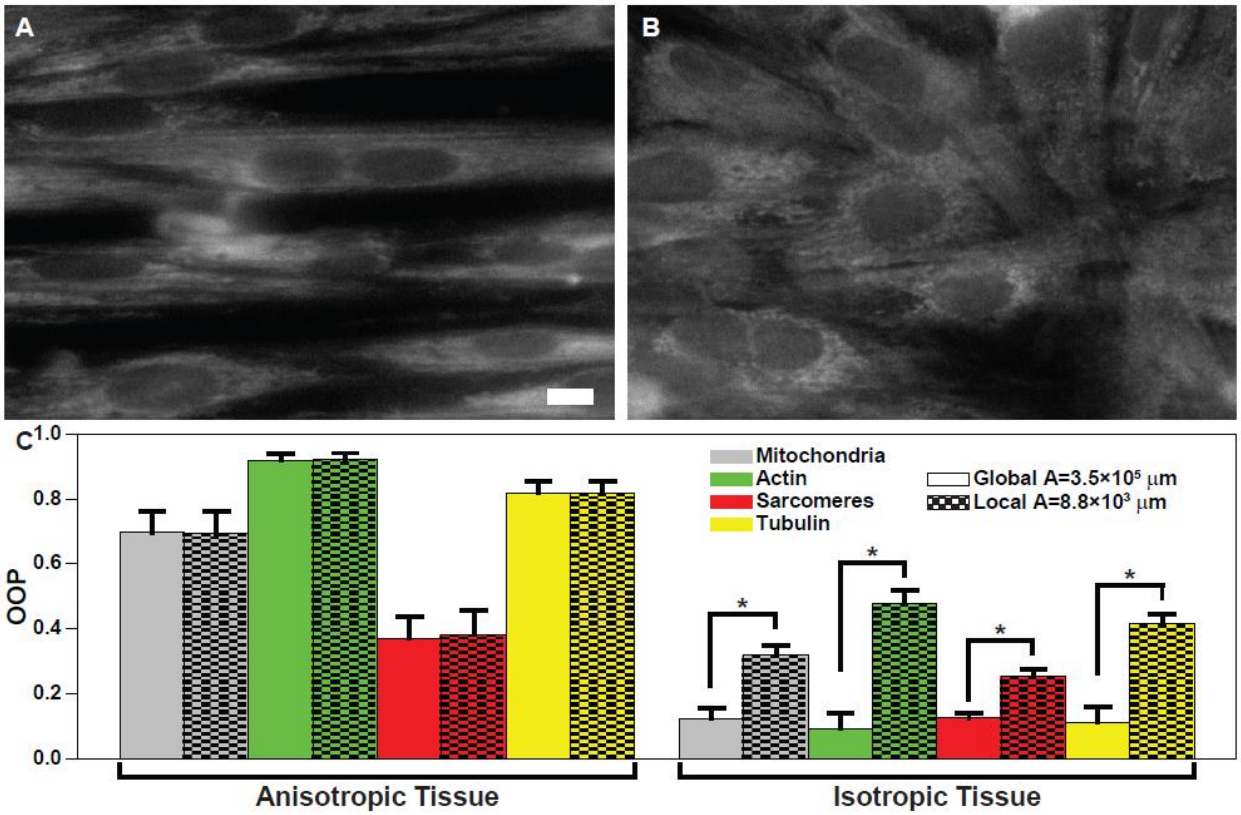

Fig. 5: OOP analysis for mitochondria compared to three other constructs. (A-B) Immunostain images of mitochondria from anisotropic (A) and isotropic (B) tissues. (C) OOP data for anisotropic and isotropic tissues over two spatial scales. Error bars represent the standard deviation of the data. Significance was tested within groups (anisotropic (Mitochondria N=12, Actin N=10, Sarcomere N=3, Tubulin N=9), isotropic (Mitochondria N=12, Actin N=12, Sarcomere N=4, Tubulin N=8)) and was $p<0.05$ where labeled with an asterisk. Scale bar 10 μm.

To test whether the fixation method used affected mitochondrial organization, live tissues stained with MitoTracker were imaged and analyzed as well (Fig. 6A-B) and compared to fixed samples (Fig. 6C(i), D(i)). The orientations detected for the mitochondria were examined to ensure that the OOP data collected previously was not a result of cell boundaries (Fig. 6C(ii), D(ii)). The orientation vectors confirm that the cell boundaries do not affect the orientation vectors. The angles of the orientation vectors also follow patterns expected of anisotropic and isotropic tissues (Fig. 6E). There appears to be a difference between the OOP values for live and fixed samples, both for anisotropic and isotropic tissues, although the difference is not quite statistically significant for the data analyzed (Fig. 6F).

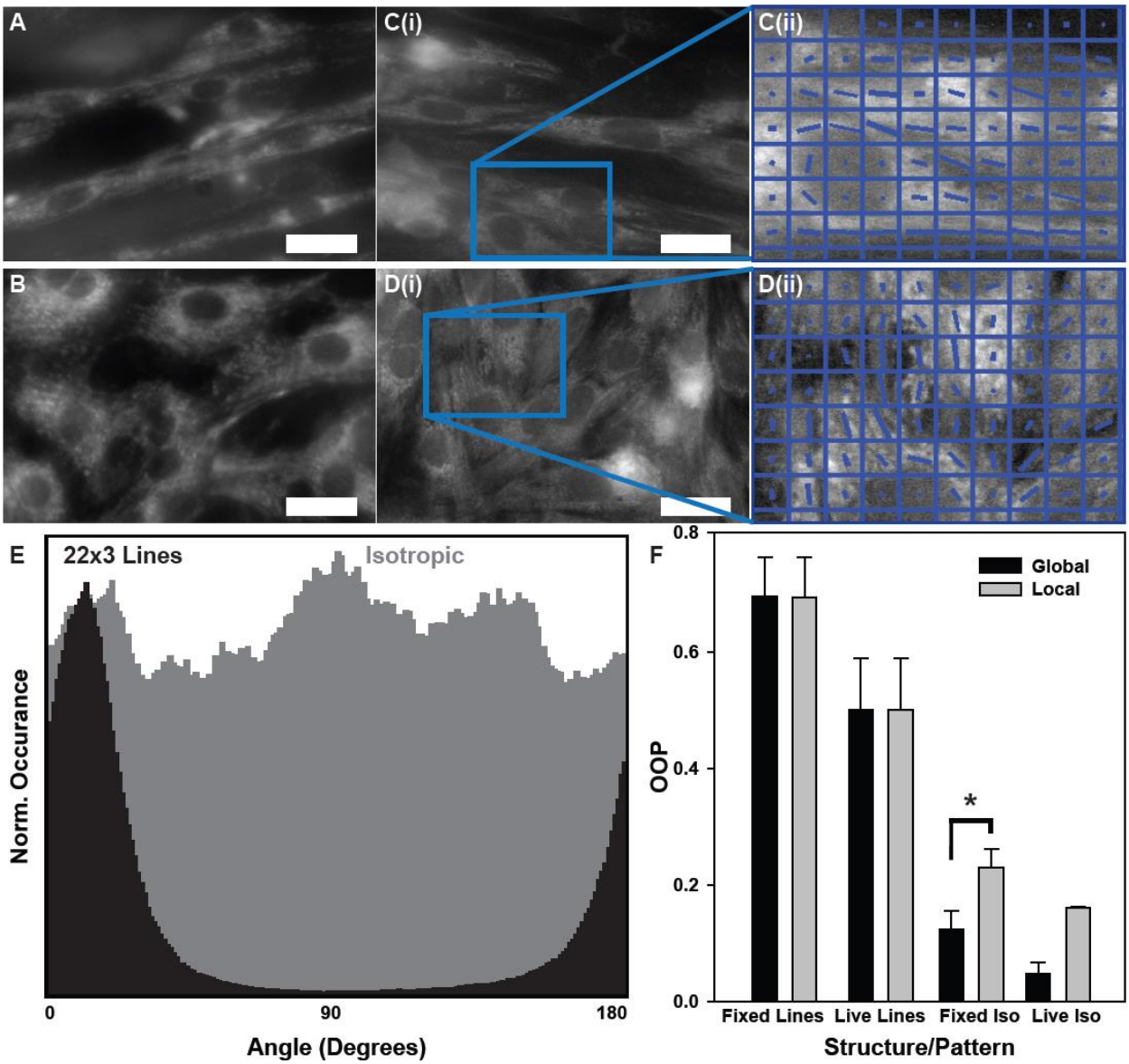

Fig. 6: Live and fixed mitochondria. (A-C(i), D(i)) Immunostain images of mitochondria from live anisotropic (A), live isotropic (B), fixed anisotropic (C(i)), and fixed isotropic (D(i)) tissues. (C(ii), D(ii)) Orientation vectors produced by construct detection code. (E) Histogram of angles of orientation vectors produced by construct detection code. (F) Preliminary OOP data for live (anistropic N=7, isotropic N=3) and fixed (anisotropic N=12, isotropic N=12) mitochondria images. Error bars represent the standard deviation of the data. Significance was tested within each tissue type (anisotropic, isotropic) and was $p<0.05$ where labeled with an asterisk. Scale bar 25 μm.

The COOP was also implemented to examine the correlations between mitochondria and the other constructs in isotropic tissues (Fig. 7). The mitochondria were found to be tightly correlated to the actin (Fig. 7 (i)), which may further suggest that the mitochondrial organization is closely linked to the cytoskeletal organization. However, it was found that they were not fully

coordinated to the sarcomeres (Fig. 7 (ii)) or the microtubules (Fig. 7 (iii)). This may be due to issues with the images and stain, as some of the mitochondria analyzed appear to have larger, rounder morphologies than others (Fig. S2). Because these morphologies can be characteristic of unhealthy mitochondria, they may not be acceptable samples for analysis. This issue was not observed with the other constructs analyzed, as images of the actin, nuclei, sarcomeres, and microtubules are of acceptable quality. Another potential issue is the noise that is apparent in the mitochondria images between cells and within the areas occupied by the nuclei (Fig. 6A-C(i), D(i), S2). This observation led to the development of the noise test conducted in Chapter 1, which shows that the noise does not affect the OOP values of other constructs (Fig. 2).

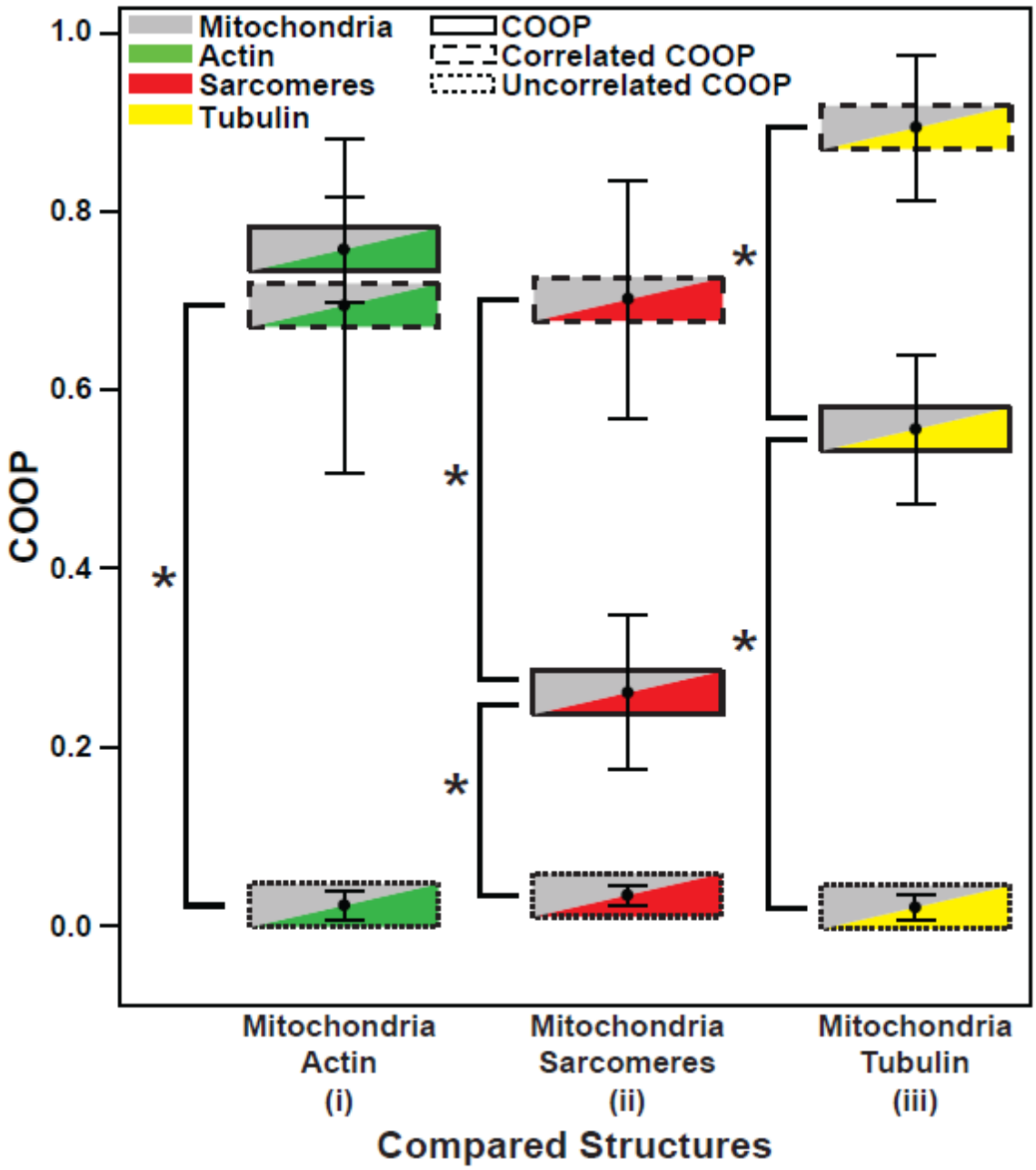

Fig. 7: COOP analysis for mitochondria against other constructs. COOP data representing correlation between mitochondria and actin (i) (N=11), sarcomeric Z-lines (ii) (N=4), and tubulin of microtubules (iii) (N=7). Error bars represent standard deviation of data. Significance was tested within each pair of constructs between the COOP, Uncorrelated COOP, and Correlated COOP, and was $p<0.05$ where labeled with an asterisk. Scale bars 10 μm.

Discussion and Future Directions

Studying the organization of mitochondria has the potential to immensely impact the structure-function relationship of energy production and consumption sites within cardiac

tissues. While these results remain to be repeated and validated, the applications of this method could provide a new basis for characterizing structure-function relationships. In the future, a more appropriate stain will be used for immunofluorescent imaging of these tissues to validate any resulting OOP and COOP analysis. In addition, the mitochondrial organization will be analyzed over multiple spatial and temporal scales for comparison with the data from Chapter 1. Understanding how mitochondrial organization and correlations are affected by changes in tissue organization may be essential for comprehending heart disease and for assessing engineered tissues and stem cell-derived tissues.

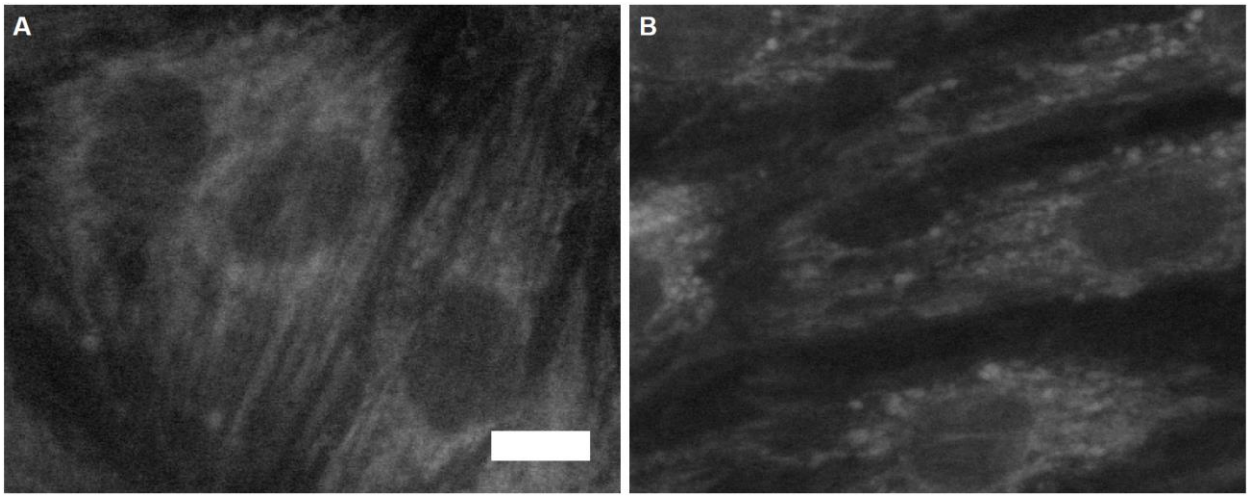

Fig. S2: Variation in mitochondria morphology. (A-B) Immunostain images of tubular (A) and round (B) mitochondria from isotropic tissues. Scale bar 10 μm.

References

1. Maron, B.J. and W.C. Roberts, *Quantitative analysis of cardiac muscle cell disorganization in the ventricular septum of patients with hypertrophic cardiomyopathy.* Circulation, 1979. **59**(4): p. 689-706.
2. Pong, T., et al., *Hierarchical architecture influences calcium dynamics in engineered cardiac muscle.* Exp Biol Med (Maywood), 2011. **236**(3): p. 366-73.
3. Grosberg, A., et al., *Self-organization of muscle cell structure and function.* PLoS Comput Biol, 2011. **7**(2): p. e1001088.
4. Bursac, N., *Cardiomyocyte Cultures With Controlled Macroscopic Anisotropy: A Model for Functional Electrophysiological Studies of Cardiac Muscle.* Circulation Research, 2002. **91**(12): p. 45e-54.
5. Du, A., J.M. Sanger, and J.W. Sanger, *Cardiac myofibrillogenesis inside intact embryonic hearts.* Dev Biol, 2008. **318**(2): p. 236-46.
6. Bray, M.A., et al., *Nuclear morphology and deformation in engineered cardiac myocytes and tissues.* Biomaterials, 2010. **31**(19): p. 5143-50.
7. Streeter, D.D., et al., *Fiber orientation in the canine left ventricle during diastole and systole.* Circulation Research, 1969. **24**(3): p. 339-347.
8. Atherton, B., D. Meyer, and D. Simpson, *Assembly and remodelling of myofibrils and intercalated discs in cultured neonatal rat heart cells.* Journal of Cell Science, 1986. **86**(1): p. 233-248.
9. Rothen-Rutishauser, B.M., et al., *Different Behaviour of the Non-sarcomeric Cytoskeleton in Neonatal and Adult Rat Cardiomyocytes.* J Mol Cell Cardiol, 1998. **30**(1): p. 19-31.
10. Sheehy, S.P., et al., *Quality metrics for stem cell-derived cardiac myocytes.* Stem cell reports, 2014. **2**(3): p. 282-294.
11. Feinberg, A.W., et al., *Controlling the contractile strength of engineered cardiac muscle by hierarchal tissue architecture.* Biomaterials, 2012. **33**(23): p. 5732-41.
12. Akins, R., et al., *Cardiac organogenesis in vitro: reestablishment of three-dimensional tissue architecture by dissociated neonatal rat ventricular cells.* Tissue engineering, 1999. **5**(2): p. 103-118.
13. LeGrice, I.J., et al., *Laminar structure of the heart: ventricular myocyte arrangement and connective tissue architecture in the dog.* American Journal of Physiology-Heart and Circulatory Physiology, 1995. **269**(2): p. H571-H582.
14. Sacks, M.S. and D.C. Gloeckner, *Quantification of the fiber architecture and biaxial mechanical behavior of porcine intestinal submucosa.* Journal of Biomedical Materials Research, 1999. **46**(1): p. 1-10.
15. Geisse, N.A., S.P. Sheehy, and K.K. Parker, *Control of myocyte remodeling in vitro with engineered substrates.* In Vitro Cell Dev Biol Anim, 2009. **45**(7): p. 343-50.
16. Drew, N.K., et al., *Metrics for Assessing Cytoskeletal Orientational Correlations and Consistency.* 2015.
17. Grosberg, A., et al., *Ensembles of engineered cardiac tissues for physiological and pharmacological study: heart on a chip.* Lab Chip, 2011. **11**(24): p. 4165-73.
18. Hong, L., Y. Wan, and A. Jain, *Fingerprint image enhancement: algorithm and performance evaluation.* Pattern Analysis and Machine Intelligence, IEEE Transactions on, 1998. **20**(8): p. 777-789.

19. Kovesi, P.D., *MATLAB and Octave functions for computer vision and image processing.* Online: http://www. csse. uwa. edu. au/~ pk/Research/MatlabFns/# match, 2000.
20. Volfson, D., et al., *Biomechanical ordering of dense cell populations.* Proc Natl Acad Sci U S A, 2008. **105**(40): p. 15346-51.
21. Sun, J., J. Tang, and J. Ding, *Cell orientation on a stripe-micropatterned surface.* Chinese Science Bulletin, 2009. **54**(18): p. 3154-3159.
22. Balachandran, K., et al., *Cyclic strain induces dual-mode endothelial-mesenchymal transformation of the cardiac valve.* Proceedings of the National Academy of Sciences, 2011. **108**(50): p. 19943-19948.
23. Umeno, A. and S. Ueno, *Quantitative analysis of adherent cell orientation influenced by strong magnetic fields.* NanoBioscience, IEEE Transactions on, 2003. **2**(1): p. 26-28.
24. Hamley, I.W., *Introduction to soft matter: synthetic and biological self-assembling materials*2013: John Wiley & Sons.
25. Aoki, H., J. Sadoshima, and S. Izumo, *Myosin light chain kinase mediates sarcomere organization during cardiac hypertrophy in vitro.* Nature medicine, 2000. **6**(2): p. 183-188.
26. Taniguchi, K., et al., *Mammalian formin fhod3 regulates actin assembly and sarcomere organization in striated muscles.* Journal of Biological Chemistry, 2009. **284**(43): p. 29873-29881.
27. Drubin, D.G., H.D. Jones, and K.F. Wertman, *Actin structure and function: roles in mitochondrial organization and morphogenesis in budding yeast and identification of the phalloidin-binding site.* Molecular Biology of the Cell, 1993. **4**(12): p. 1277-1294.
28. Bissell, M.J., et al., *Tissue structure, nuclear organization, and gene expression in normal and malignant breast.* Cancer Research, 1999. **59**(7 Supplement): p. 1757s-1764s.
29. Weiss, P., *Experiments on cell and axon orientation in vitro: the role of colloidal exudates in tissue organization.* Journal of Experimental Zoology, 1945. **100**(3): p. 353-386.
30. Schliwa, M., *Mechanisms of intracellular organelle transport*, in *The cytoskeleton*1984, Springer. p. 1-82.
31. Saks, V.A., et al., *Intracellular energetic units in red muscle cells.* Biochemical Journal, 2001. **356**(Pt 2): p. 643-657.
32. Segretain, D., A. Rambourg, and Y. Clermont, *Three dimensional arrangement of mitochondria and endoplasmic reticulum in the heart muscle fiber of the rat.* The Anatomical Record, 1981. **200**(2): p. 139-151.
33. Seppet, E.K., et al., *Functional complexes of mitochondria with Ca,MgATPases of myofibrils and sarcoplasmic reticulum in muscle cells.* Biochimica et Biophysica Acta (BBA) - Bioenergetics, 2001. **1504**(2–3): p. 379-395.
34. Seppet, E.K., et al., *Intracellular energetic units in healthy and diseased hearts.* Experimental & Clinical Cardiology, 2005. **10**(3): p. 173-183.
35. Vendelin, M., et al., *Mitochondrial regular arrangement in muscle cells: a "crystal-like" pattern*. Vol. 288. 2005. C757-C767.
36. Birkedal, R., H.A. Shiels, and M. Vendelin, *Three-dimensional mitochondrial arrangement in ventricular myocytes: from chaos to order*. Vol. 291. 2006. C1148-C1158.

37. Osellame, L.D., T.S. Blacker, and M.R. Duchen, *Cellular and molecular mechanisms of mitochondrial function.* Best Practice & Research Clinical Endocrinology & Metabolism, 2012. **26**(6): p. 711-723.
38. Korzeniewski, B., *Regulation of ATP supply during muscle contraction: theoretical studies.* Biochem. j, 1998. **330**: p. 1189-1195.
39. Bessman, S. and P. Geiger, *Transport of energy in muscle: the phosphorylcreatine shuttle.* Science, 1981. **211**(4481): p. 448-452.